# A Wash-Free Homogeneous Colorimetric Immunoassay Method

Huiqiao Liu[1,⊥], Pengfei Rong[2,⊥], Hongwei Jia[3,⊥], Jie Yang[1], Bo Dong[1], Qiong Dong[2], Cejun Yang[2], Pengzhi Hu[2], Wei Wang[2], Haitao Liu[3], Dingbin Liu*[,1]

[1] College of Chemistry, Research Center for Analytical Sciences, State Key Laboratory of Medicinal Chemical Biology, Tianjin Key Laboratory of Molecular Recognition and Biosensing, and Collaborative Innovation Center of Chemical Science and Engineering, Nankai University, 94 Weijin Road, Tianjin 300071, China

[2] Department of Radiology, The Third Xiangya Hospital, Central South University, Changsha, Hunan 410013, China

[3] Key Laboratory of Optical Information Science and Technology, Ministry of Education, Institute of Modern Optics, Nankai University, Tianjin 300071, China

*E–mail: liudb@nankai.edu.cn.

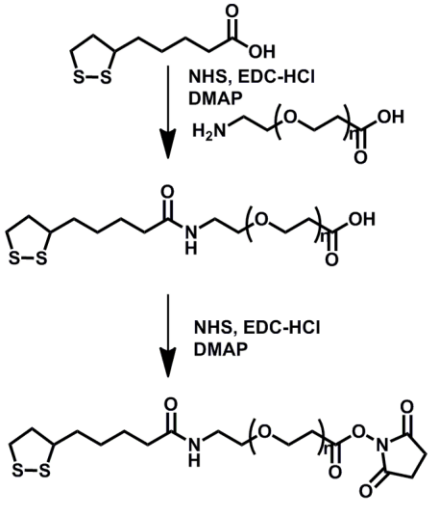


**Scheme S1.** Synthesis of the PEG linker whose one side is thioctic acid and the other side is terminated in *N*-hydroxysucinimide (NHS)-activated carboxylic acid. (DMAP is the catalyst)

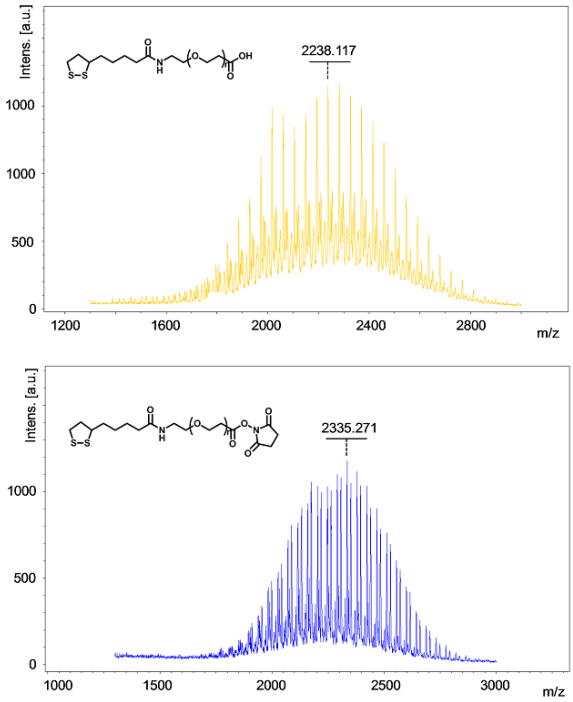


**Figure S1.** MALDI-TOF-MS data for the intermediate product and the final product indicated in **Scheme S1**.

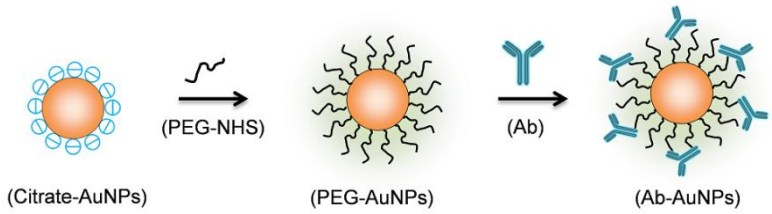


**Figure S2.** The preparation protocol of antibody (Ab)-functionalized AuNPs starting from citrate-stabilized AuNPs.

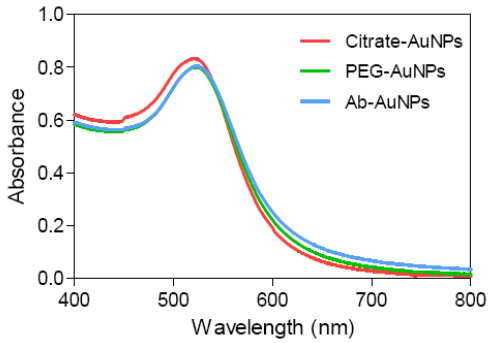


**Figure S3.** UV-vis absorption spectra of citrate-AuNPs, PEG-AuNPs, and Ab-AuNPs. The graduate red-shift of the absorption bands indicates the success of the step-by-step functionalization shown in Figure S2.

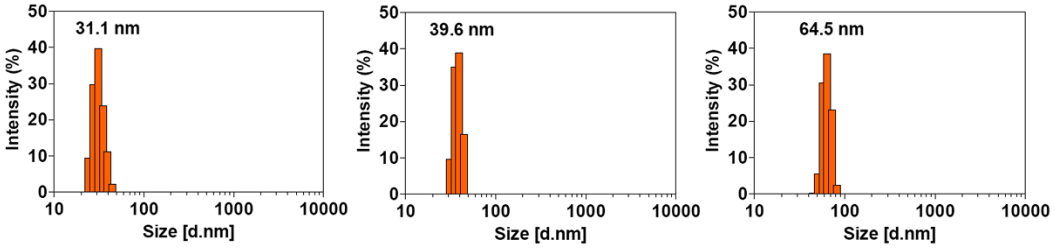


**Figure S4.** DLS measurements for citrate-AuNPs, PEG-AuNPs, and Ab-AuNPs.

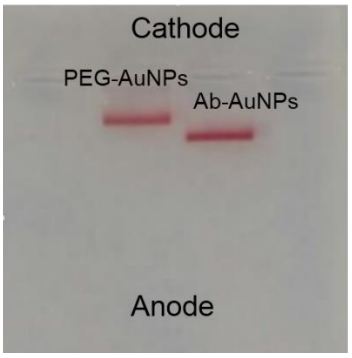


**Figure S5.** Gel electrophoresis measurement for PEG-AuNPs and Ab-AuNPs.

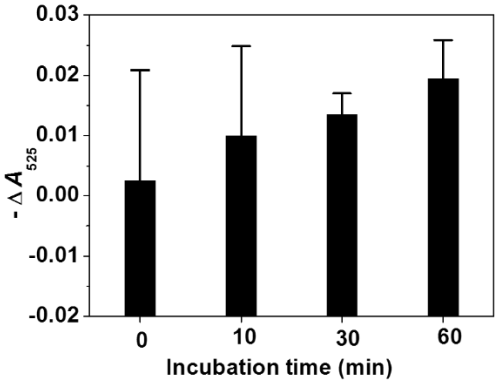


**Figure S6.** Histogram of $-\Delta A_{525}$ versus different incubation times of Ab-AuNPs and 100 ng/ml of IgG. $-\Delta A_{525} = A - A_0$, where $A$ is the absorbance of Ab-AuNP incubate with IgG for different time at 525 nm after adding Au growth solutions, and $A_0$ is that adding Au growth solution to Ab-AuNP and IgG mixture before incubation. The error bars represent the standard deviations of three independent measurements.

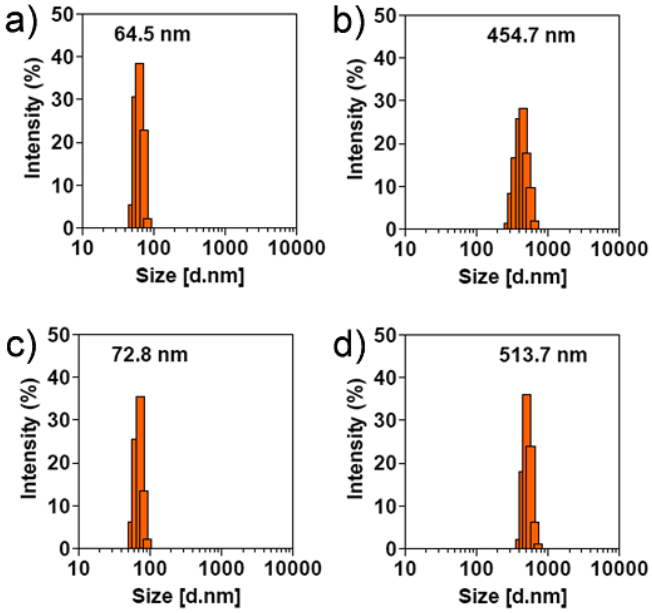


**Figure S7.** DLS measurements for the AuNPs samples. a) Ab-AuNPs; b) Ab-AuNPs incubated with target protein (human IgG, 100 ng/mL); c) Ab-AuNPs added with Au growth solutions ($NH_2OH$ (20 mM) and $HAuCl_4$ (120 μM)); d) The target protein-treated Ab-AuNPs added with the Au growth solutions. The concentration of Ab-AuNPs is 0.5 nM.

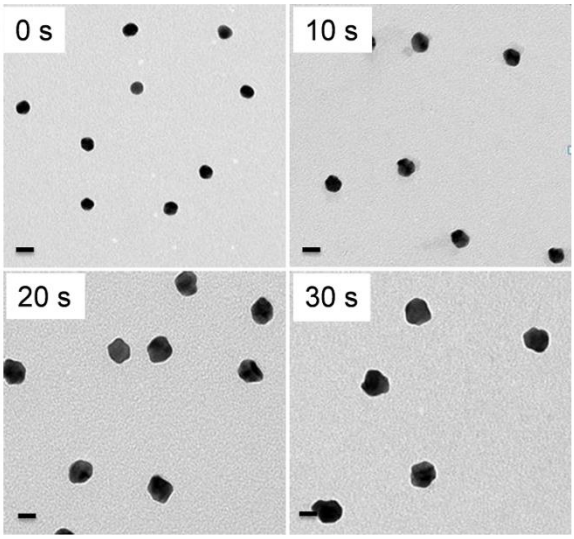


**Figure S8.** TEM images of the Ab-AuNP intermediates prepared by stopping the nanoparticle growth with mercaptopropionic acid (2 mM) after 0, 10, 20, and 30 s of the reaction.

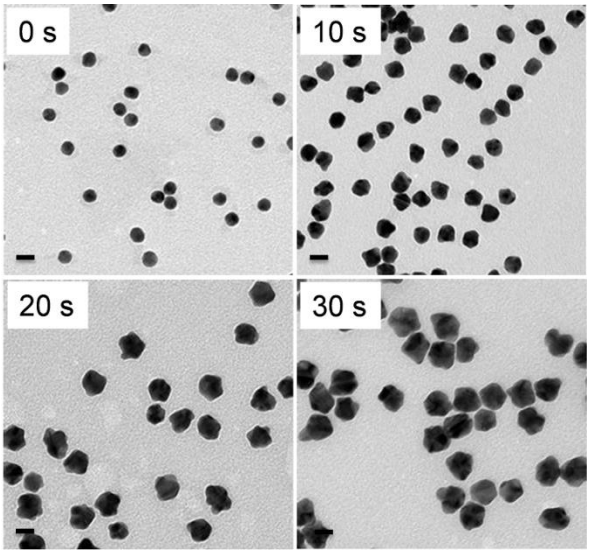


**Figure S9.** TEM images of the Ab-AuNP intermediates in the presence of detection target and the AuNP solutions were prepared by stopping the nanoparticle growth with mercaptopropionic acid (2 mM) after 0, 10, 20, and 30 s of the reaction.

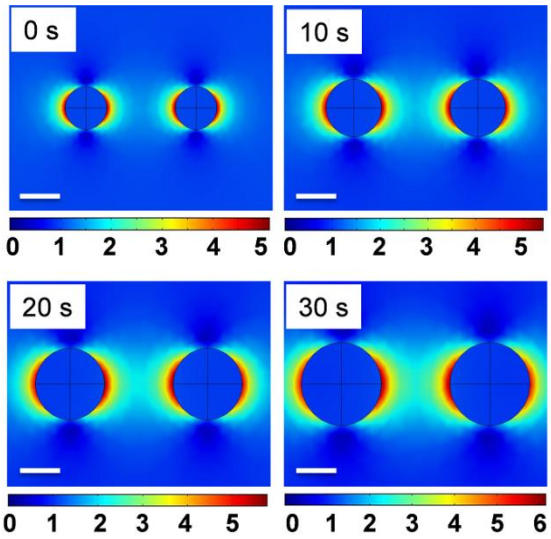


**Figure S10.** Near-field distributions of the normalized electric field ($|\mathbf{E}|/|\mathbf{E}_{inc}|$) of AuNPs corresponding to various radii of the AuNPs after 0, 10, 20, and 30 s in Figure S6. The excitation wavelength of the laser is 633 nm. The scale bars are 15 nm.

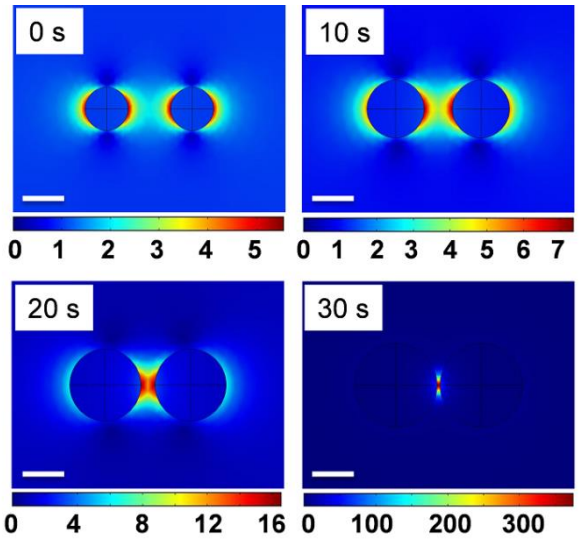


**Figure S11.** Near-field distributions of the normalized electric field ($|\mathbf{E}|/|\mathbf{E}_{inc}|$) of AuNPs corresponding to the radii of the AuNPs after 0, 10, 20, and 30 s in Figure S7. The excitation wavelength of the laser is 633 nm. Stronger field enhancement is achieved since the width of the gap becomes smaller. The scale bars are 15 nm.

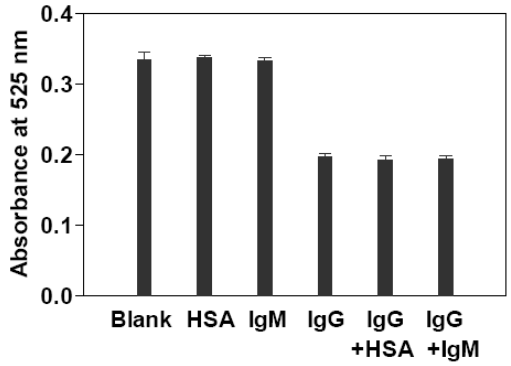


**Figure S12.** Specificity of the AuNP-based colorimetric immunoassay for IgG. The concentrations of each protein are prepared to be 100 ng/mL. The error bars represent the standard deviations of three independent measurements.

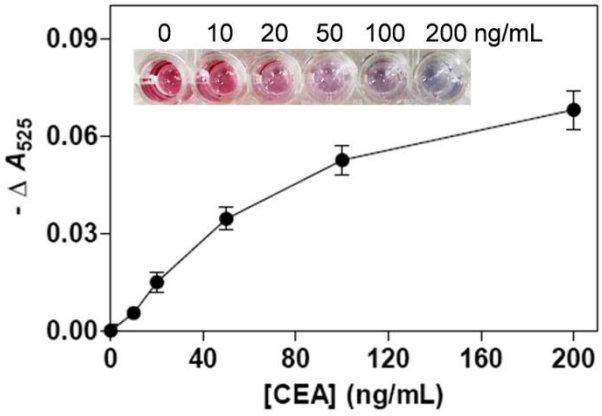


**Figure S13.** Plots of $-\Delta A_{525}$ versus various concentrations of cancer biomarker CEA as well as corresponding color change in the AuNPs samples. Error bars show the standard deviations of three independent measurements.

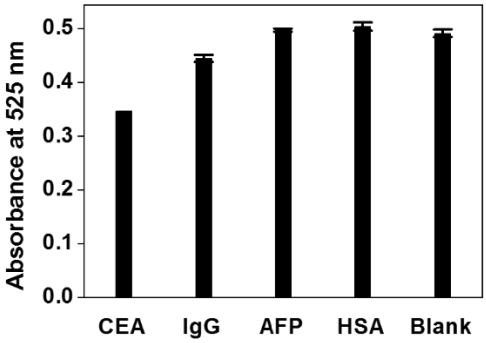


**Figure S14.** Specificity of the AuNP-based colorimetric immunoassay for CEA. The concentrations of each protein are prepared to be 100 ng/mL. The error bars represent the standard deviations of three independent measurements.

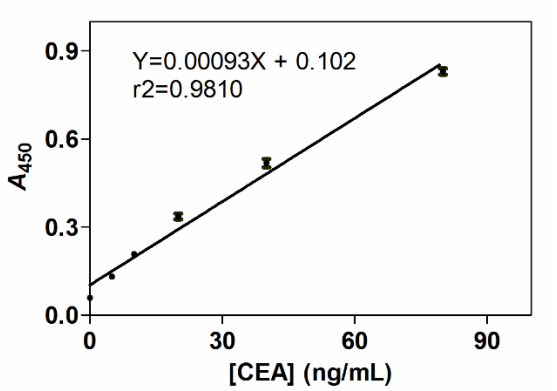


**Figure S15.** HRP-based ELISA for the detection of various concentrations of CEA spiked in fetal bovine sera. The OD values at 450 nm were recorded by a conventional microplate reader. Error bars show the standard deviations of three independent measurements.

**Table S1.** Comparison of normalized electric-field magnitude and intensity for different sized mono-dispersed AuNPs.

| Particle size | $\max\|\mathbf{E}\|/\|\mathbf{E}_{inc}\|$ | $\max\|\mathbf{E}\|^2/\|\mathbf{E}_{inc}\|^2$ |
|---|---|---|
| 15 nm | 5.11 | 26.11 |
| 20 nm | 5.4 | 29.16 |
| 25 nm | 5.76 | 33.18 |
| 29 nm | 6.15 | 37.82 |

**Table S2.** Comparison of normalized electric-field magnitude and intensity in the nano-gap for AuNPs oligomers composed of different sized AuNPs.

| Particle size | $\max\|\mathbf{E}\|/\|\mathbf{E}_{inc}\|$ | $\max\|\mathbf{E}\|^2/\|\mathbf{E}_{inc}\|^2$ |
|---|---|---|
| 15 nm | 5.55 | 30.80 |
| 20 nm | 7.34 | 53.88 |
| 25 nm | 16.3 | 265.69 |
| 29 nm | 336 | $1.13\times10^5$ |

**Table S3.** Comparison of AuNP-based immunoassays for various detection targets.

| target | nanomaterial | linear range | detection limit | real sample | ref |
|---|---|---|---|---|---|
| RIgG | AuNRs | 0-20 ng/ml | 1.5 ng/ml | N/A | S1 |
| IgG | Au-patterning nanostructures | N/A | 66.7 pM | N/A | S2 |
| CEA | AuNPs | 0-120 ng/ml | 3 ng/ml | serum | S3 |
| IgG | Au Nanoclusters | 0.1-400 ng/ml | 0.04 ng/mL | serum | S4 |
| PSA | AuNPs | $1.11\times10^{3}$-$1.11\times10^{7}$ aM | 111aM | N/A | S5 |
| IgG | Au nanoplates | N/A | 10 pg/mL | N/A | S6 |
| CRP | AuNPs | N/A | 50 ng/mL | serum | S7 |
| PSA and p24 | AuNPs | N/A | $10^{-18}$ g/mL | serum | 11 |
| AFP | AuNPs | 0.1-5.0 ng/mL | 0.01 ng/mL | serum | S8 |
| AFP | gold-coated magnetic nanoparticle | N/A | 0.01 ng/mL | N/A | S9 |
| P53 | AuNPs | N/A | 5 pg/mL | N/A | S10 |
| IgG | AuNPs | 0 -100 ng/mL | 3.74 ng/mL | N/A | This study |
| CEA | AuNPs | 0 -100 ng/mL | 5.66 ng/mL | serum | This study |

**Table S4.** The $-\Delta A_{525}$ values using the proposed AuNP-based colorimetric immunoassay for the clinical samples collected from 6 healthy individuals and 18 patients suffering from cancer.

| Healthy | | Cancer | | | | | |
|---|---|---|---|---|---|---|---|
| Patient ID | $-\Delta A_{525}$ | Patient ID | $-\Delta A_{530}$ | Patient ID | $-\Delta A_{525}$ | Patient ID | $-\Delta A_{530}$ |
| 401543 | 0.002± 0.001 | 401546 | 0.033± 0.0045 | 378416 | 0.018± 0.005 | 379668 | 0.023± 0.002 |
| 400578 | 0.001± 0.003 | 401542 | 0.026± 0.0048 | 396435 | 0.015± 0.002 | 391794 | 0.022± 0.0055 |
| 401588 | 0.001± 0.006 | 402971 | 0.051± 0.006 | 390360 | 0.002± 0.0008 | 398770 | 0.028± 0.004 |
| 341426 | -0.008± 0.002 | 254757 | 0.014± 0.0047 | 401020 | -0.02± 0.0001 | 401090 | 0.011± 0.001 |
| 401596 | -0.03± 0.002 | 389433 | 0.029± 0.0055 | 386163 | -0.015± 0.00045 | 303556 | 0.029± 0.002 |
| 401155 | 0.003± 0.0008 | 210843 | 0.050± 0.002 | 401259 | 0.004± 0.0003 | 399281 | 0.030± 0.002 |

**Table S5.** Clinical information of the 6 healthy individuals.

| Sample No. | Patient ID | Age | Sex |
|---|---|---|---|
| A1 | 401543 | 45 | Male |
| A2 | 400578 | 60 | Male |
| A3 | 401588 | 50 | Male |
| A4 | 341426 | 80 | Male |
| A5 | 401596 | 66 | Male |
| A6 | 401155 | 23 | Female |

**Table S6.** Clinical information of the 18 patients suffering from various types of cancer and their diagnostic results by the clinical standard strategies and conventional ELISA.

| Sample No. | Patient ID | Age | Sex | Diagnosis | CEA level (ng/mL) |
|---|---|---|---|---|---|
| B1 | 401546 | 75 | Male | Rectal Carcinoma | 55.2 |
| B2 | 401542 | 59 | Male | Lung Carcinoma | 48.5 |
| B3 | 402971 | 61 | Male | Osteocarcinoma | 86.8 |
| B4 | 254757 | 48 | Female | Breast Carcinoma | 6.8 |
| B5 | 389433 | 46 | Male | Colon Carcinoma | 35.2 |
| B6 | 210843 | 51 | Female | Colon Carcinoma | 92.5 |
| C1 | 378416 | 56 | Female | Breast Carcinoma | 15.3 |
| C2 | 396435 | 56 | Female | Ovarian Carcinoma | 25.0 |
| C3 | 390360 | 65 | Female | Breast Carcinoma | Undetectable |
| C4 | 401020 | 58 | Male | Lung Carcinoma | Undetectable |
| C5 | 386163 | 57 | Male | Pancreatic Head Carcinoma | Undetectable |
| C6 | 401259 | 69 | Male | Hepatocirrhosis | Undetectable |
| D1 | 379668 | 61 | Male | Colon Carcinoma | 28.3 |
| D2 | 391794 | 68 | Male | Colon Carcinoma | 34.5 |
| D3 | 398770 | 78 | Male | Lung Carcinoma | 45.0 |
| D4 | 401090 | 50 | Male | Anal Carcinoma | 8.4 |
| D5 | 303556 | 66 | Male | Colon Carcinoma | 35.8 |
| D6 | 399281 | 48 | Female | Hysterocarcinoma | 32.9 |

**Reference**

S1. Gao ZQ, Deng KC, Wang XD, Miro M, Tang DP. High-resolution colorimetric assay for rapid visual readout of phosphatase activity based on gold/silver core/shell nanorod. ACS Appl Mater Interfaces. 2014; 6: 18243−50.

S2. Hsu CY, Huang JW, Lin KJ. High sensitivity and selectivity of human antibody attachment at the interstices between substrate-bound gold nanoparticles. Chem Commun. 2011; 47: 872–74.

S3. Luo C, Wen W, Lin FG, Zhang XH, Gu HS and Wang SF. Simplified aptamer-based colorimetric method using unmodified gold nanoparticles for the detection of carcinoma embryonic antigen. RSC Adv. 2015; 5: 10994–9.

S4. Liu HY, Wu XM, Zhang X, Burda C, Zhu JJ. Gold nanoclusters as signal amplification labels for optical immunosensors. J Phys Chem C. 2012; 116: 2548–54.

S5. Truong PL, Cao C, Park S, Kim M, Sim SJ. A new method for non-labeling attomolar detection of diseases based on an individual gold nanorod immunosensor. Lab Chip. 2011; 11: 2591−97.

S6. Beeram SR, Zamborini FP. Purification of gold nanoplates grown directly on surfaces for enhanced localized surface plasmon resonance biosensing. ACS Nano. 2010; 4: 3633−46.

S7. Kitayama Y, Takeuchi T. Localized surface plasmon resonance nanosensing of C-Reactive Protein with poly(2-Methacryloyloxyethyl Phosphorylcholine)-grafted gold nanoparticles prepared by surface-initiated atom transfer radical polymerization. Anal Chem. 2014; 86: 5587−94.

S8. Bi S, Yan YM, Yang XY, Zhang SS. Gold nanolabels for new enhanced

chemiluminescence immunoassay of alpha-fetoprotein based on magnetic beads. Chem Eur J 2009; 15: 4704–9.

S9. Chun C, Joo J, Kwon D, Kim CS , Cha HJ, Chung MS and Jeon S. A facile and sensitive immunoassay for the detection of alpha-fetoprotein using gold-coated magnetic nanoparticle clusters and dynamic light scattering. Chem Commun. 2011; 47: 11047–9.

S10. Jia CP, Zhong XQ, Hua B, Liu MY, Jing FX, Lou XH, Yao SH, Xiang JQ, Jin QH, Zhao JH. Nano-ELISA for highly sensitive protein detection. Biosens Bioelectron. 2009; 24: 2836–41.